

Phase Transformation and Deformation Model for Quenching Simulations

Y. Kaymak

VDEh Betriebsforschungsinstitute GmbH, Düsseldorf, NW, Germany

Introduction

In materials science, quenching is the rapid cooling of a workpiece to obtain certain material properties. For instance, quenching can reduce the crystal grain size of metallic materials and increasing their hardness. The rapid cooling prevents undesired phase transformations from occurring by reducing the window of time during which these undesired phase transformations are thermodynamically and kinetically favorable.

The process of steel quenching is a progression, beginning with heating the sample up to a precise temperature, which is between 815°C and 900°C for the most of the steel types. The temperatures throughout the workpiece should be kept as uniform as possible during the heating. Afterwards, the workpiece is rapidly cooled usually by soaking in a fluid bath. Similar to the heating step, it is important that the temperature throughout the sample remains as uniform as possible during soaking. Often, the workpiece is excessively hard and brittle after quenching. In some cases, one or more tempering process steps are performed additionally in order to increase the toughness. In a tempering sub-process, the quenched steel is heated up to some critical temperature for a certain period of time, and then allowed to cool. The typical temperature evolution during the heat treatment process is show in Figure 1.

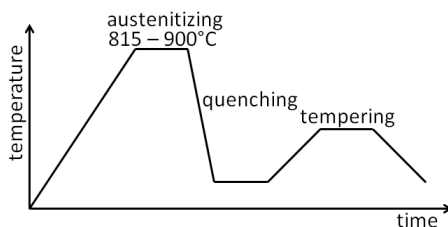


Figure 1. Temperature evolution during a typical heat treatment process.

Heat treatment of the advanced steel grades (like micro-alloyed steels or AHSS steel grades) is a challenging process as the residual stress/deformation are pronounced and the quality requirements of the customers are getting tighter. A comprehensive modelling of the complex phenomena to estimate the

residual stress and deformation is essential for developing an optimal process control. The basis of the complex quenching model presented in this paper is developed within author's PhD thesis [1]. The model consists of a series of coupled physics, which are summarized in Figure 2. These coupled fields are solved by using the physics interfaces in COMSOL Multiphysics®. The temperature field is solved by the heat transfer in solids physics. The micro-structure field is modelled using kinetic expressions and domain ODEs and DAE physics. The displacement field is solved using the solid mechanics physics including the volume change (due to the temperature and micro-structure changes), plasticity, transformation induced plasticity (trip), creep, and large deformations. The constitutive model parameters as well as the isothermal and martensitic transformation kinetic parameters are validated and calibrated by several dilatometry tests.

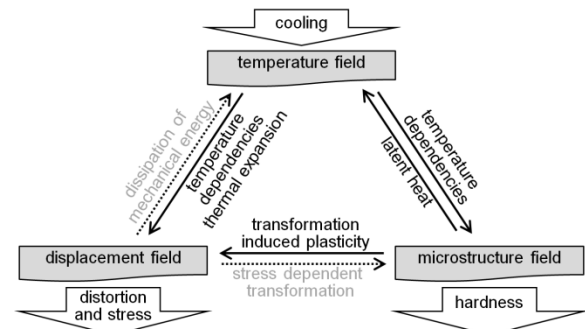


Figure 2. Coupling of fields in quenching process.

Theory and Governing Equations

The quenching simulation model is focused on the cooling since the most significant part of the residual stress and deformation is developed during this rapid cooling. The model presented here consists of strongly coupled phenomena of heat transfer, micro-structure change, deformation (due to the thermal shrinkage, microstructure change related dilatation, trip, creep, plasticity, and large deformations). The governing fields involved in the quenching process and their interactions are shown in Figure 2. In quenching, the temperature field is controlled by the cooling boundary conditions. The temperature

evolution drives the phase transformation kinetics and phase transformations are accompanied by latent heat release. Moreover, all the material properties depend on the temperature and microstructure. A linear mixture rule is used for the Young's modulus E , Poisson's ratio ν , initial yield stress σ_{y0} , heat capacity C_p and thermal conductivity k . However, a harmonic mixture rule is used for the density ρ .

$$\begin{aligned} E &= f_a E_a(T) + f_b E_b(T) + f_m E_m(T) \\ \nu &= f_a \nu_a(T) + f_b \nu_b(T) + f_m \nu_m(T) \\ \sigma_{y0} &= f_a \sigma_{ay0}(T) + f_b \sigma_{by0}(T) + f_m \sigma_{my0}(T) \\ C_p &= f_a C_{pa}(T) + f_b C_{pb}(T) + f_m C_{pm}(T) \\ k &= f_a k_a(T) + f_b k_b(T) + f_m k_m(T) \\ \rho &= \frac{1}{\frac{f_a}{\rho_a(T)} + \frac{f_b}{\rho_b(T)} + \frac{f_m}{\rho_m(T)}} \end{aligned}$$

where the subscripts a , b and m correspond to the austenite, bainite and martensite microstructure volume fractions. T stands for the temperature and f represents the volume fraction of the microstructure. For the sake of simplicity a perfectly plastic behavior can be assumed if needed.

The heat generation due to dissipation of mechanical energy has no significant influence on the temperature field. Similarly, the stress dependency of the transformations can also be discarded. So, these two coupling phenomena greyed-out in Figure 2. The temperature field is solved by the heat transfer in solids physics in COMSOL Multiphysics® software. The micro-structure field is modelled at integration point level using kinetic expressions and domain ODEs and DAE physics. The displacement field is solved using the solid mechanics physics including the volume change due to the temperature and micro-structure changes. This volumetric strain is given by:

$$dL = \sqrt[3]{\frac{\rho_a(T_{\text{ref}})}{\rho}} - 1$$

where T_{ref} is the strain reference temperature ρ_a is the austenite density and ρ is the mixture density. It is assumed that initial microstructure is completely austenite. Moreover, the nonlinear phenomena like plasticity, transformation induced plasticity (trip), creep, and large deformations are also considered in the solid mechanics physics setup in COMSOL. The governing partial differential equations (PDEs) and expressions of the model are further discussed on the following sub-sections.

Temperature field:

The temperature field in solid material is modelled by the heat transfer in solids physics:

$$\begin{aligned} \rho C_p \frac{\partial T}{\partial t} + \nabla \cdot \mathbf{q} &= Q \\ \mathbf{q} &= -k \nabla T \end{aligned}$$

where, ρ is the density, C_p is the heat capacity, T is temperature field, t is the time, \mathbf{q} is heat flux vector, k is the heat conductivity, Q heat source due to the latent heat of the phase transformations. The equation for the heat source Q depends on the transformation latent heats as well as the phase transformation rates. It is defined by:

$$Q = L_{ab} \dot{f}_b + L_{am} \dot{f}_m$$

where, L_{ab} and L_{am} are the latent heats of the austenite to bainite and austenite to martensite transformations, \dot{f}_b and \dot{f}_m are the rates of the austenite to bainite and austenite to martensite transformations, respectively.

For the sake of simplicity, the temperature field in the quenching medium is not modelled. Instead, either the temperature or heat flux at the solid boundaries are defined, e.g., by using convective heat transfer coefficients and radiation to ambient.

Microstructure field:

There are two types of transformations relevant to this study: (1) austenite to bainite transformation, which is diffusion controlled, needs an incubation time before the transformation starts. (2) Austenite to martensite transformation, which is diffusionless, is controlled only by temperature that means it can be expressed as a function of temperature without solving or integration a PDE.

The austenite to bainite transformation is modelled using the domain ODEs. The transformation kinetics for the bainite formation is assumed to obey the Scheil's addition rule and Johnson-Mehl-Avrami-Kolmogorow (JMAK) equation. Two state variables per integration point are defined, one for the Scheil's sum and the other for bainite volume fraction in JMAK-equation. The Scheil's sum ss is obtained by integrating:

$$ss = \frac{1}{Bs(T)}$$

The incubation time is completed when the Scheil's sum reaches the unity. After this incubation time, the

bainite volume fraction f_b is obtained by integrating JMAK-equation:

$$\dot{f}_b = K \cdot n \cdot t^{n-1} \cdot \exp(-K \cdot t^n)$$

where, n is known as JMAK-exponent and K is JMAK-factor. They are calculated using the bainite transformation start time $Bs(T)$ and finish time $Bf(T)$. These start and finish curves are given in the Time-Temperature-Transformation (TTT) diagrams. If it is assumed that the bainite volume fraction f_b is 0.01 at the starting time and 0.999 at the finishing time, JMA-exponent n and the JMAK-factor K are calculated by:

$$n = \frac{-\ln\left(\frac{\ln(1-0.01)}{\ln(1-0.999)}\right)}{\ln(Bf(T)) - \ln(Bs(T))}$$

$$K = \frac{\ln(1-0.01)}{\ln(Bs(T)^n)}$$

The martensite transformation is described by the Koistinen-Marburger equation (KM) equation, which does not require any additional PDEs to solve or integrate. It is assumed that martensite forms below the martensite start temperature M_s and the martensite volume fraction f_m only depends on the temperature T by the expression:

$$f_m = 1 - \exp(-0.011(M_s - T))$$

Displacement field:

The displacement field in solid material is modelled by the solid mechanics physics. Since the governing PDEs are quite complex, they are not all re-written here. All the material properties are temperature and microstructure dependent as given in the initial paragraph of the theory and governing equations. The volume expansion due to density changes is included using the volumetric strain expression dL . The inelastic strains due to the transformation induced plasticity (trip) and creep are defined using the initial stress/strain feature in COMSOL Multiphysics®. The calculation of inelastic strains is described in detail in the following sub-section.

Model for trip and creep:

The inelastic strains due to transformation induced plasticity (trip) and creep are volume conserving and proportional to the stress deviator. The components of the symmetric inelastic strain tensor ec_{ij} are defined as state variables per integration point. These components of the inelastic strain tensor are integrated from the inelastic strain rate expressions:

$$\dot{ec}_{ij} = (A_{tr} + A_{cr}) \cdot n_{ij}^S$$

where, n_{ij}^S describes the unit direction of stress deviator, A_{tr} defines the transformation induced plasticity part of the inelastic strain rate and A_{cr} defines the creep rate. Additionally an effective inelastic strain ec_{eff} is also defined similar to the effective plastic strain in the von Mises plasticity. The effective inelastic strain is integrated from:

$$ec_{eff} = \sqrt{\frac{2}{3} \sum ec_{ij}^2}$$

So in total seven state variables (ec_{11} , ec_{22} , ec_{33} , ec_{12} , ec_{13} , ec_{23} , ec_{eff}) are defined and stored per integration point. These state variables are integrated at each integration point using the domain ODEs.

In its classical definition, trip is the significantly increased plasticity during a phase change even if the macroscopic equivalent stress is smaller than the yield stress of the material. The trip part of the inelastic strains A_{tr} is described by the Greenwood–Johnson (GJ) mechanism. The Greenwood–Johnson mechanism corresponds to the micromechanical plastic strain arising in the parent phase (e.g., austenite) from the expansion of the product phases (e.g., martensite and bainite). It is proportional to the rate of transformation and the effective stress:

$$A_{tr} = \{K_b^{GJ} \cdot \dot{f}_b \cdot \ln(f_b) + K_m^{GJ} \cdot \dot{f}_m \cdot \ln(f_m)\} \cdot \sigma_{eff}$$

where, K_b^{GJ} and K_m^{GJ} are Greenwood–Johnson trip constants for bainite and martensite, respectively. To avoid numerical problems with the logarithm of zero phase fractions, this equations is applied once a certain threshold phase fraction is formed, e.g., 3%.

The creep induced part of the inelastic strains A_{cr} is described by the Norton's creep law:

$$A_{cr} = \left(\frac{\sigma_{eff}}{\sigma_{ref}(T)}\right)^{n_{cr}(T)}$$

where σ_{eff} is the effective stress, $\sigma_{ref}(T)$ is a material specific temperature dependent creep reference stress, and similarly $n_{cr}(T)$ is also a material specific temperature dependent creep exponent. In the context of this paper, the simplest creep equation (Norton's creep law) is presented. However, more sophisticated creep models can be adopted easily just by replacing the creep rate expression A_{cr} .

Simulation Results

A series of dilatometry measurements are performed within the study. In this paper, the results of simulation model for two selected dilatometry test are presented. The experimental and calculated values fit quite well with each other. A typical geometry of the dilatometry specimen is shown Figure 3. The specimen is fixed in the dilatometry device using the two holes at its ends. The region of interest is the narrow middle region of the specimen. The dilatometry device is programmed to apply a given temperature and mechanical loading sequence. The specimen temperature T is continuously monitored using a contact thermocouple as well as the relative displacement ΔL of the notches of the specimen.

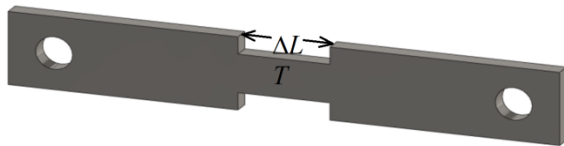


Figure 3. Typical dilatometry specimen geometry.

The simulation model geometry is simplified by skipping the holes, which have negligible influence on the region of interest which is the narrow section at the middle of the specimen. Moreover, only the one eighth of the remaining geometry is modelled by taking the advantage of the 3 symmetry planes. The modelled geometry and its mesh are shown Figure 4.

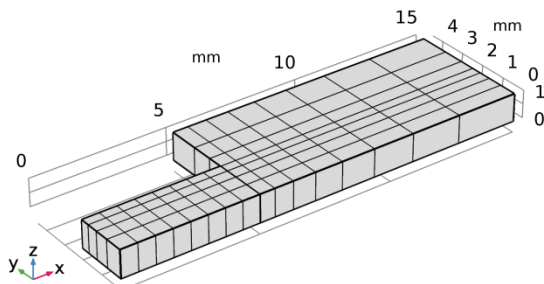


Figure 4. Model geometry and its mesh.

Two selected dilatometry test are simulated with the model to assess the capabilities (1) creep dominated high temperature behavior and (2) transformation induced plasticity (trip) dominated behavior.

Creep behavior:

The first case study is for the creep dominant deformation at high temperature, i.e. at 750°C. The specimen is rapidly cooled from 850°C to 750°C. Then, an initial tensile stress of 80MPa is applied and the specimen kept at that temperature until it fails due to creep. The measured temperature and computed average temperature over the volume of interest

region are given in Figure 5. There is almost a perfect match in measured and computed temperatures since the measured temperature is set on some boundaries as boundary condition.

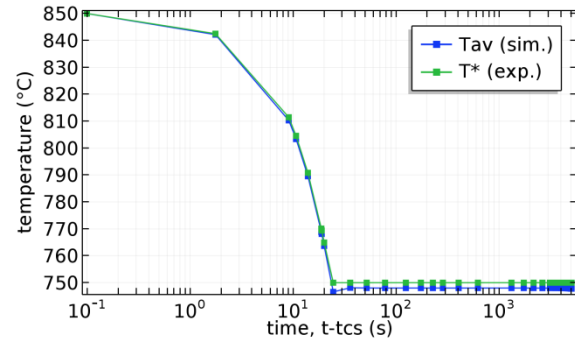


Figure 5. Temperature history in creep test.

Although a constant load is applied, the introduced initial tensile stress of 80MPa increases as the cross-sectional area is contracted. Finally, the specimen ruptures at the middle, the area with maximum contraction. The evolution of the average stress through the middle cross-sectional area during the creep test is shown in Figure 6.

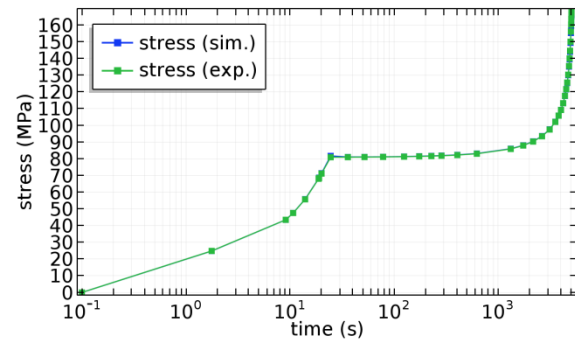


Figure 6. Stress history in creep test.

The experimentally observed strain and simulation model computed strains are compared in Figure 7. The red curve shows the strain in experiment, which is computed using the measured displacement ΔL between the notches of the specimen and the initial distance $\Delta L_0 = 10\text{mm}$. This is done by assuming the stress state is uniaxial and uniform in between, which is not fully correct. Therefore, two curves for the model calculated strains are shown for comparison. The blue curve shows the average engineering strain over the cross-section at the middle of the specimen. The green curve is something similar to what is done in experiment: the relative average displacement at the notches divided by the initial distance 10mm. The main reasons for the differences between these curves are on one side the crude assumption of the strain estimation and on the other side the weakness of the

Norton's creep law. Since the Norton's creep law is the simplest among the creep laws, its capability to describe the complete creep evolution is very limited. Nonetheless, the model results are consistent with the dilatometry tests and satisfactorily good for the intended usage of the model.

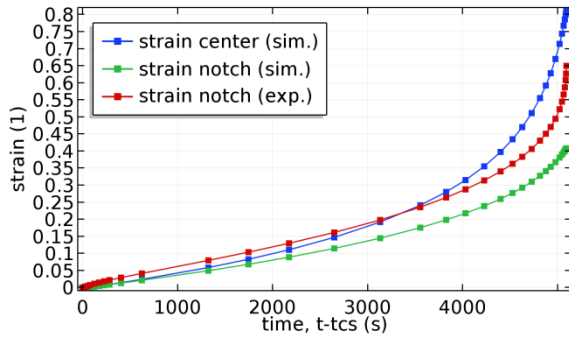


Figure 7. Strain history in creep test.

The effective stress field in the specimen just before the creep failure is shown in Figure 8. The necking at the middle obviously explains how the cross-sectional area is contracted and the true stress is increased even under a constant applied load. The initial 80MPa tensile stress rises up to 166MPa during the necking indication more than 50% area reduction.

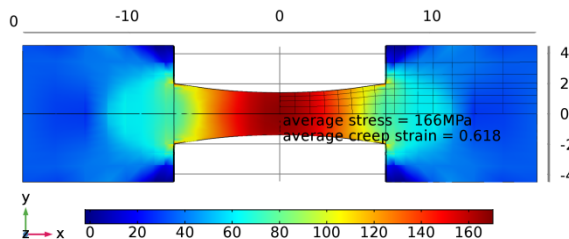


Figure 8. Stress field just before creep failure.

Trip behavior:

The second case study is for the transformation induced plasticity. The specimen is first rapidly cooled from 850°C to approximately 300°C. Then, a constant load is applied, which produces 20MPa tensile stress meanwhile the specimen kept at constant temperature. After an incubation time, the austenite to bainite transformation starts and finally completes. The measured and computed temperatures are given in Figure 9. As before in creep test, there is a perfect match between measured and computed temperatures. The stress evolution during the trip test is shown in Figure 10. Although the applied load introduces just 20MPa, which is far smaller than the yield stress, additional plastic deformation occurs during the phase transformations, which is the focus of the trip study case. The results related to the trip

phenomenon will be further explained in the following text and figures.

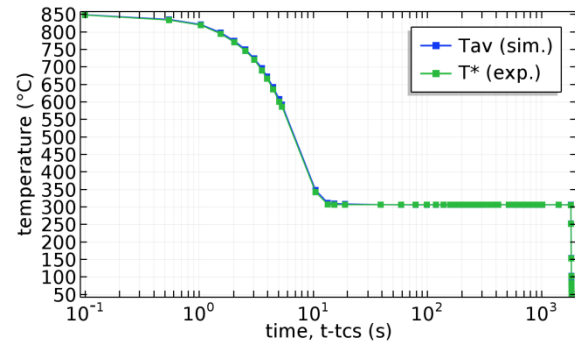


Figure 9. Temperature history in trip test.

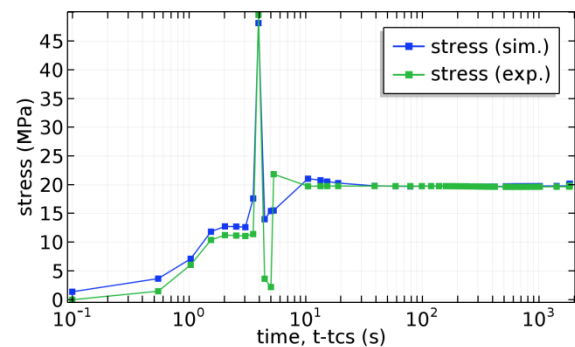


Figure 10. Stress history in trip test.

The experimentally observed strain and simulation model computed strains are compared in Figure 11. Similar to the creep test, the red and green curves show the strain in experiment and simulation model, which are computed using the notch displacement of the specimen. The relative notch displacement is directly measured in the experiment by using a strain gauge. The blue curve in Figure 12 shows this experimentally measured displacement. Horizontal axis represents the complete time line including the heating phase at the beginning of the experiment. The green curve with circles shows the average relative notch displacement computed by the model. The model starts with the cooling at *tcs* (time of cooling start). The initial contraction occurs due to thermal shrinkage. Afterwards, an expansion occurs even if the temperature is constant. This expansion is due to the volume expansion during the austenite to bainite transformation combined with the transformation induced plasticity (trip). The blue curve (Figure 11) shows the average engineering strain over the cross-section at the middle of the specimen. The strains computed by the model are in good agreement with the experimentally observed strain.

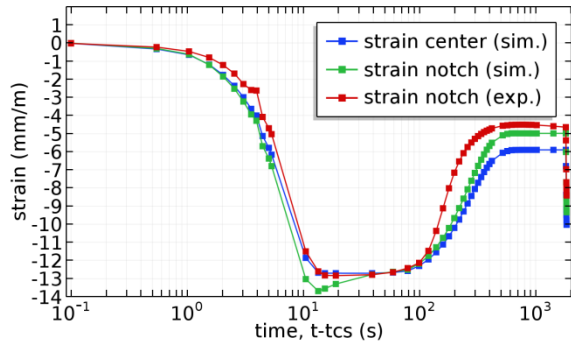


Figure 11. Strain history in trip test.

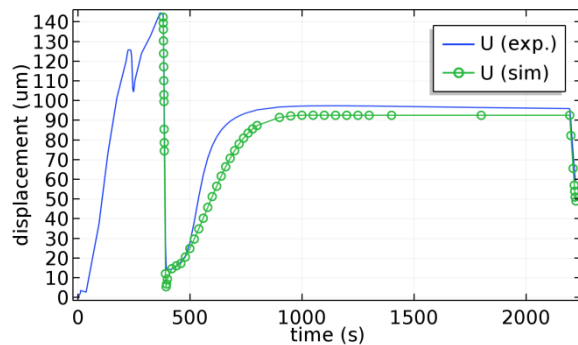


Figure 12. relative notch displacement in trip test.

The thermal shrinkage during the cooling, and the elongation due to phase transformation dilatation and trip during constant temperature can be better distinguished in the temperature-strain relation as shown in Figure 13. The jump is due to dilatation and trip during the austenite to bainite isothermal phase transformation. The linear parts represent the thermal shrinkage of austenite at higher temperatures and bainite at lower temperatures.

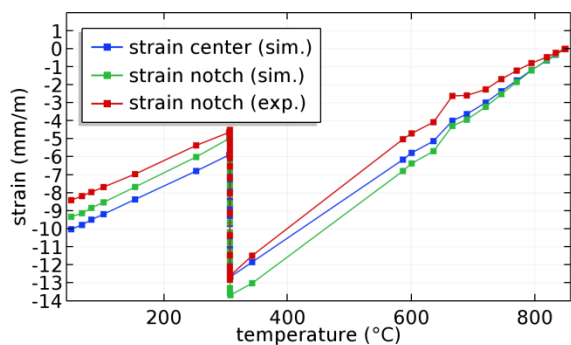


Figure 13. Strain-temperature relation in trip test.

Figure 14 summarizes phase transformation related data. The solid curves without markers are ferrite start, pearlite start, pearlite finish, bainite start and bainite finish curves, respectively. These curves are just shown as info for referencing the literature curves. The curves with markers are used in the

simulation model as input. The yellow curve with stars is the volume averaged temperature over the region of interest (narrow middle region of the specimen). The black curve with circles and blue curve with diamonds are martensite start and finish temperatures, respectively. The green curve with squares and red curve with pluses are bainite start and finish curves, respectively.

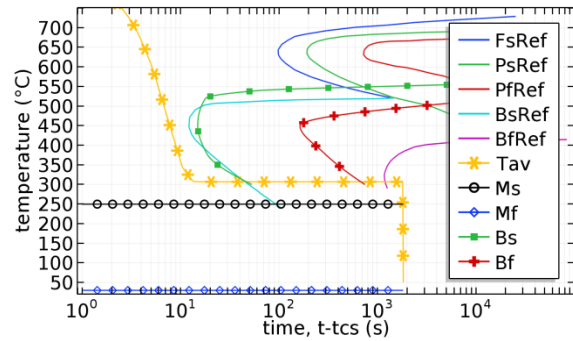


Figure 14. TTT diagram and cooling curve.

The evolutions of the Scheil's sum and the microstructures are shown in Figure 15. The volume average of the Scheil's sum ss is the blue curve with stars, when it reaches the unity, then it means the incubation time is complete and the austenite to bainite transformation starts. The volume average of the bainite volume fraction f_b is plotted by the green curve with circles. As the bainite forms, the austenite (f_a the turquoise curve with squares) is equally consumed. There is no martensite (f_m red curve with diamonds) formation since all the austenite was transformed into bainite prior to the martensite start temperature M_s .

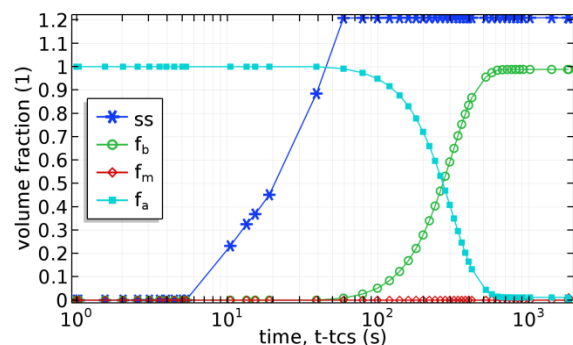


Figure 15. Evolutions of the Scheil's sum and the microstructures.

Conclusions

A complex model for the simulation of the quenching process has been introduced, which can be used in the heat treatment simulation of the advanced steel grades to compute the residual stress and deformation

as well as the microstructure. The introduced model consists of a series of coupled physics. The temperature, microstructure and displacement fields are solved by considering dilatation and nonlinear phenomena (plasticity, trip, creep, and large deformations). The constitutive model parameters as well as the isothermal and martensitic transformation kinetic parameters are validated and calibrated by several dilatometry tests.

The development of the model is still in progress. As a next step, this model will be applied to the simulation of the process line, where the strips are continuously heat treated. With the help of the simulations, the heat treatment processes control can be optimized to meet the customer requirements with minimal material waste.

References

1. Y. Kaymak, *PhD Thesis: Simulation of Metal Quenching Processes for the Minimization of Distortion and Stresses*, pages 17-25, Otto von Guericke University, Magdeburg (2007)

Acknowledgements

The work presented here has been carried out with a financial grant from the Research Fund for Coal and Steel (RFCS) of the European Community with grant agreement no: RFSR-CT-2015-00012 and project title "*Optimal Residual Stress Control*" (ORSC).

Furthermore, the author greatly acknowledges the support from the company "Hugo Vogelsang GmbH & Co. KG", especially Mr. Andreas Heßler and his colleges who supplied the test specimens as well as the research institute "Instytut Metalurgii Żelaza im. Stanisława Staszica", especially Prof. Roman Kuziak and his colleges who carried out the dilatometry tests. In addition, the author gratefully acknowledges the intensive cooperation among the project partners and author's colleges Mr. Fabien Nkwitchoua and Mr. Volker Diegelmann.